OPEN ACCESS

REPORT

Mercury evidences link intensive volcanism to the Late Ordovician mass extinction and changes in the atmosphere-land-ocean system

Zhen Qiu,[1,2,*] Weiliang Kong,[1] Jiaqiang Zhang,[1,3] David B. Kemp,[4] Qin Zhang,[1] Wen Liu,[1] Stephen E. Grasby,[5] and Caineng Zou[1,2]

*Correspondence: qiuzhen316@163.com

Received: October 27, 2024; Accepted: January 23, 2025; Published Online: February 18, 2025; https://doi.org/10.59717/j.xinn-geo.2024.100124

GRAPHICAL ABSTRACT

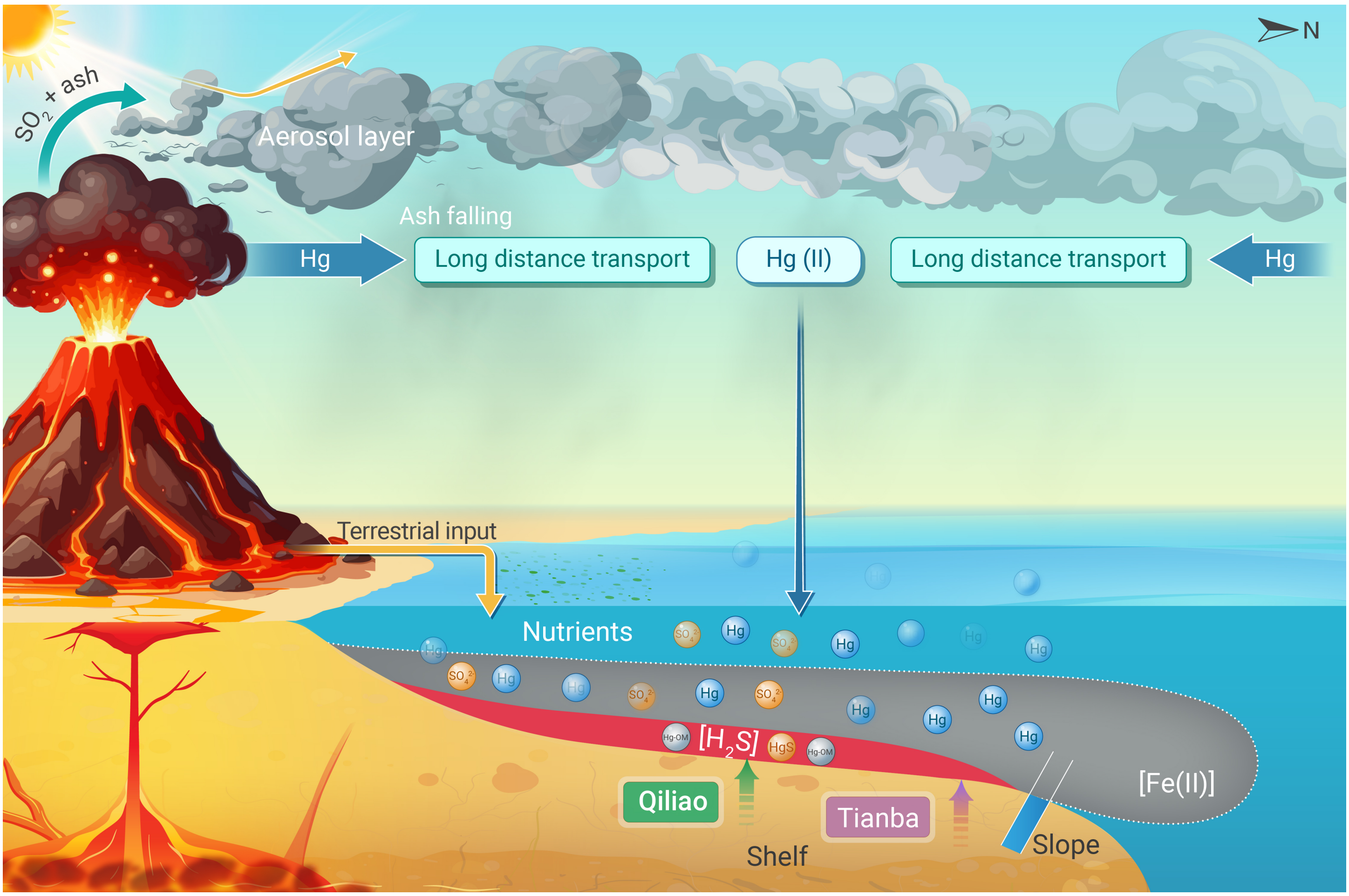

PUBLIC SUMMARY

- Organic matter and sulfides are both important hosts of Hg during the Late Ordovician Mass Extinction.
- Hg isotopes across the Ordovician-Silurian transition indicate multiple Hg sources linked to volcanism.
- Intensive volcanism induced significant changes in the atmosphere-land-ocean system.

REPORT

Mercury evidences link intensive volcanism to the Late Ordovician mass extinction and changes in the atmosphere-land-ocean system

Zhen Qiu,[1,2,*] Weiliang Kong,[1] Jiaqiang Zhang,[1,3] David B. Kemp,[4] Qin Zhang,[1] Wen Liu,[1] Stephen E. Grasby,[5] and Caineng Zou[1,2]

[1]Research Institute of Petroleum Exploration & Development, China National Petroleum Corporation, Beijing 100083, China

[2]School of Geoscience and Technology, Southwest Petroleum University, Chengdu 610500, China

[3]State Key Laboratory of Lithospheric Evolution, Institute of Geology and Geophysics, Chinese Academy of Sciences, Beijing 100029, China

[4]State Key Laboratory of Biogeology and Environmental Geology and Hubei Key Laboratory of Critical Zone Evolution, School of Earth Sciences, China University of Geosciences (Wuhan), Wuhan 430074, China

[5]Geological Survey of Canada, Natural Resources Canada, Calgary, Alberta T2L 2A7, Canada

*Correspondence: qiuzhen316@163.com

Received: October 27, 2024; Accepted: January 23, 2025; Published Online: February 18, 2025; https://doi.org/10.59717/j.xinn-geo.2024.100124

Citation: Qiu Z., Kong W., Zhang J., et al. (2025). Mercury evidences link intensive volcanism to the Late Ordovician mass extinction and changes in the atmosphere-land-ocean system. *The Innovation Geoscience* **3**:100124.

The Late Ordovician mass extinction (LOME, ca. 445 Ma), which occurred over two extinction intervals (LOMEI-1 and LOMEI-2), was the first "Big Five" biotic crises of the Phanerozoic. The ultimate trigger of this extinction remains debated, with glacially induced global cooling and volcanism-driven warming events separately suggested as the underlying cause. Here, we report anomalously high mercury (Hg) levels in two Ordovician-Silurian successions from a shelf-to-slope transect in South China, indicating abnormally high Hg loading to the ocean. Analyses of Hg isotopes through the successions reveal near-zero Δ^{199}Hg from the late Katian to the earliest Hirnantian (LOMEI-1), suggesting that Hg was mainly derived from large-scale volcanism. Positive shifts in Δ^{199}Hg are observed during the Hirnantian stage, coincident with global glaciation, suggesting enhanced Hg sequestration to sediments driven by subsidence of cold and dense surface seawater. Negative shifts in Δ^{199}Hg values across the LOMEI-2 within the Hirnantian likely suggest enhanced terrestrial Hg and sulfate fluxes to the ocean due to volcanism-induced global warming, which promoted oceanic anoxic/euxinic conditions. This study provides novel evidences linking intensive volcanism to significant changes in the atmosphere-land-ocean system across the Ordovician-Silurian transition, particularly to the euxinic ocean conditions that triggered the LOME.

INTRODUCTION

The Late Ordovician Mass Extinction (LOME) saw the extinction of 53% to 85% of marine species, making it as the first and one of the greatest mass extinctions of the Phanerozoic.[1-3] The LOME occurred in two intervals, with the first interval (LOMEI-1) around the Katian/Hirnantian boundary and the second interval (LOMEI-2) in the late Hirnantian.[4,5] Expanded marine anoxia and/or euxinia has been generally invoked as one of kill mechanisms for these two extinction intervals.[6] However, the ultimate trigger of the LOME remains debated, with some models attributing to large-scale cooling,[7] and others suggesting a global warming that potentially linked to the emplacement of an unknown large igneous province (LIP).[8]

LIPs are widely regarded as a key trigger of catastrophic environmental changes responsible for mass extinction in Earth's history.[9] However, no robust evidence supports an LIP emplacement event coeval with the LOME.[8] Indirect evidence for large-scale volcanism exists in the form of anomalous high mercury (Hg) concentrations in sedimentary successions during the Ordovician-Silurian (O-S) transition (Figure 1).[8,10-13] Large-scale volcanism could emit massive amounts of Hg into the atmosphere, where long-range atmospheric transport allows them enter into global ecosystems via atmospheric deposition, resulting in anomalously high Hg concentrations in sediments worldwide.[14,15] The enrichment of Hg in sedimentary rocks may also occur via other mechanisms, however, and recent work that noted high Hg concentrations across the O-S in South China attributed Hg enrichment to intense deposition of seawater Hg under euxinic conditions, rather than to volcanism.[16] Indeed, seawater deoxygenation has been implicated as a key kill mechanism during the two pulses of LOME.[17,18] Even so, a potential link between large-scale volcanism and its possible role in driving ocean euxinia has not been fully considered in these studies.

Mercury isotopes can be used to unravel the cause of Hg enrichments in O-S successions. Mercury isotopes display large mass-dependent fractionation (MDF, normally reported in delta notation as δ^{202}Hg, see Methods) during various physical, chemical and biological processes, and large mass-independent fractionation (MIF, normally reported as Δ^{199}Hg, see Methods) during photochemical processes.[19] Since MIF of Hg isotopes is resistant to other processes, the Δ^{199}Hg values of sedimentary rocks can be used as a source tracer.[19] Volcanically derived Hg displays near-zero Δ^{199}Hg values.[20] However, the photoreduction process on Earth's surface results in negative Δ^{199}Hg values in terrestrial reservoirs (e.g., soil and vegetation) and positive Δ^{199}Hg values in marine reservoirs (e.g., sediments and seawater).[21]

Near-zero to slightly positive Δ^{199}Hg values across O-S successions have been reported recently,[11,13,16,22] providing evidence of enhanced deposition of volcanic- and seawater-derived Hg input during the LOME. However, there is still lack of high-resolution Hg isotope records, which could unravel the precise pattern of changes in Hg inputs from volcanism or other sources before, during, and after LOMEI-1 and LOMEI-2. Consequently, the link between volcanism, as inferred from mercury evidence, and LOME intervals remains unresolved. To address this, high-resolution Hg isotope analyses were conducted on two Ordovician-Silurian sections along a shelf-to-slope transect in South China. Results indicate that large-scale volcanism induced significant changes in the climate-land-ocean system and associated biotic crises during the LOME.

MATERIALS AND METHODS

Geological background and samples

During the O-S transition, the South China Block was located near the equator (Figure 1A). The Yangtze region of South China was a shallow carbonate platform during the early-mid Katian, which evolved into a siliciclastic-dominated shelf environment (Yangtze Shelf Sea) during the late Katian as a consequence of the Kwangsian Orogeny.[24,25] Black shales of the Wufeng and Lungmachi formations were widely deposited across the shelf.[26-29] The rapid sea-level fall related to the Hirnantian glaciation is indicated by the development of shallow-water, carbonate-rich deposits, known as the Kuanyinchiao Bed.[24] Abundant volcanic ash layers were deposited across the O-S transition (Figure 2), with the first episode occurring in the late Katian[25,31,32] and a second episode around the Rhuddanian–Aeronian boundary.[30,31,33]

A total of 111 fresh samples were collected from the Qiliao (QL, mid shelf) and the Tianba (TB, outer shelf) sections on the Yangtze Shelf (Figures 1B-C). In both sections, volcanic ash layers spanning the late Katian to Rhuddanian stages have been identified, as well as abundant graptolites allowing a high-resolution biostratigraphy to be constructed.[23,31] Detailed petrological information of the two sections is provided in Figures S1-S2. High-resolution data on total organic carbon (TOC), total sulfur (TS), and total Hg (THg) concentrations for the QL and TB sections have been previously reported.[23,31] High-resolution Hg isotopic data for these two sections were generated in this study (Tables S1-S2).

Hg isotopic composition analyses

Hg isotopes were analyzed using a Neptune Plus multi-collector inductively coupled plasma mass spectrometer.[34] Prior to analysis, the samples

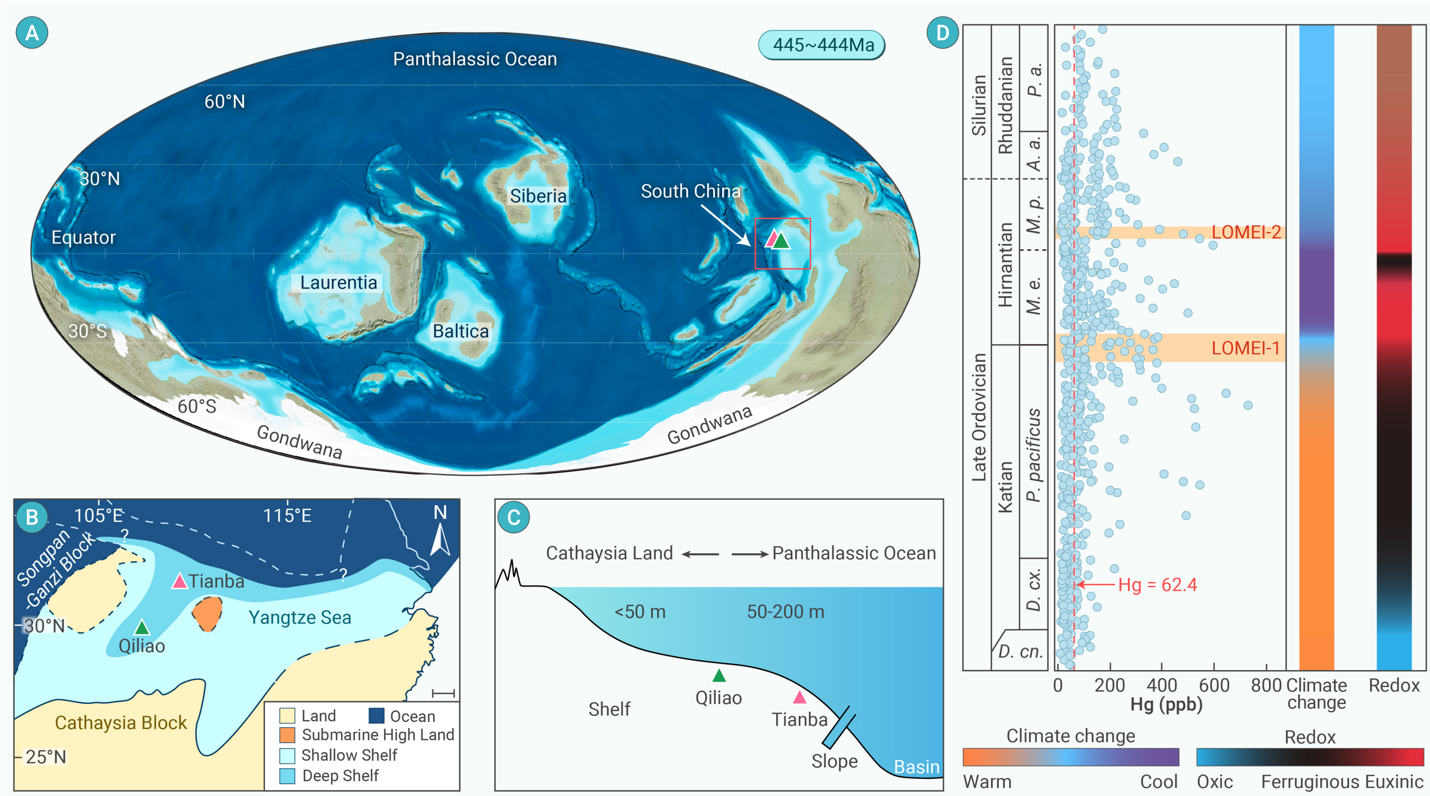

Figure 1. Geological setting (A) Late Ordovician (ca. 445~444 Ma) paleogeography. The base map is from Ron Blakey, © 2016 Colorado Plateau Geosystems Inc. (B) Simplified paleogeographic map of the Yangtze Shelf Sea during the Late Ordovician,[18] showing the locations of the Qiliao (QL) and Tianba (TB) sections. (C) Schematic cross-section of the Late Ordovician Yangtze Shelf Sea showing estimated relative paleo-depths of the studied sections.[18] Scale bar = 100 km. (D) Compiled Hg concentration data, climate change and redox condition information during the O-S transition. Hg concentrations are from refs.[10,11,13,16,22,23] Climate change and redox conditions are from refs.[6,18] The age of each sample is calculated by linear regression based on the ages of graptolite zones.[3] Graptolite zones: *D. cn.—Dicellograptus complanatus; D. cx.—Dicellograptus complexus; P. pacificus—Paraorthograptus pacificus; M. e.—Metabolograptus extraordinarius; M. p.—Metabolograptus persculptus; A. a.—Akidograptus ascensus; P. a.—Parakidograptus acuminatus.*

were pretreated using a dual-stage combustion furnace to preconcentrate Hg from the samples.[35] The Hg preconcentrated solutions were diluted to 1.0 ng/mL Hg for Hg isotope analysis. A standard (GSS-4) was prepared the same way as the samples. Mass-dependent fractionation (MDF) of Hg isotopes was reported as δ^{202}Hg notation in units of ‰ referenced to the NIST-3133 Hg standard (analyzed before and after each sample):

$$\delta^{202}\mathrm{Hg}(‰)=[(^{202}\mathrm{Hg}/^{198}\mathrm{Hg}_{sample})/(^{202}\mathrm{Hg}/^{198}\mathrm{Hg}_{standard})-1]\times 1000$$

Mass-independent fractionation (MIF) is reported in Δ notation, which describes the difference between the measured δ^{xxx}Hg and the theoretically predicted δ^{xxx}Hg value, in units of ‰:

$$\Delta^{xxx}\mathrm{Hg}=\delta^{xxx}\mathrm{Hg}\text{-}\ \delta^{202}\mathrm{Hg}\times\beta$$

Where β is 0.2520 for ^{199}Hg, 0.5024 for ^{200}Hg, and 0.7520 for ^{201}Hg.[36] The overall average and uncertainty of repeat GSS-4 analyses (δ^{202}Hg: -1.60 ± 0.10 ‰, Δ^{199}Hg: -0.53 ± 0.07 ‰, Δ^{200}Hg: -0.07 ± 0.07 ‰; Δ^{201}Hg: -0.52 ± 0.06 ‰; 2SD, n=4) agree well with previous results.[20] The analytical uncertainty of GSS-4 is used to determine the precision of the sample analyses.

RESULTS

High-resolution Hg isotopes (quantified as δ^{202}Hg and Δ^{199}Hg) were obtained from fresh samples of the QL and TB sections in South China. Five intervals can be defined in these two sections based on biostratigraphic correlation of graptolite zones. The average ± 2SD values of δ^{202}Hg, and Δ^{199}Hg were calculated to highlight the general geochemical features of the five intervals (Figure 2).

Interval I represents the early to late Katian stage (*Dicellograptus complantus* and *Paraorthograptus pacificus* graptolite zones), with data showing negative δ^{202}Hg and near-zero to slightly positive Δ^{199}Hg values at QL (-0.84 ± 0.46‰ and 0.12 ± 0.13‰, respectively) and TB (-0.97 ± 0.81‰ and 0.04 ± 0.10 ‰, respectively). Interval II corresponds to the LOMEI-1 (top of *Paraorthograptus pacificus* graptolite zone to the lower part of *Metabolograptus extraordinarius* graptolite zone). The data in this interval show negative δ^{202}Hg and near-zero to slightly positive Δ^{199}Hg values at QL (-0.25 ± 0.62‰ and 0.11 ± 0.07‰, respectively) and TB (-0.56 ± 1.07‰ and 0.06 ± 0.07‰, respectively), similar to those in Interval I. Interval III represents the peak Hirnantian glaciation (the upper part of *Metabolograptus extraordinarius* graptolite zone) and shows negative δ^{202}Hg and positive Δ^{199}Hg values at QL (-0.24 ± 0.40‰ and 0.12 ± 0.05‰, respectively) and TB (-0.52 ± 0.91‰ and 0.13 ± 0.09‰, respectively). Interval IV corresponds to the LOMEI-2 (the base of *Metabolograptus persculptus* graptolite zone) and has negative δ^{202}Hg and slightly negative to near-zero Δ^{199}Hg values at QL (-0.45 ± 0.77‰ and 0.00 ± 0.13‰, respectively) and TB (-0.48 ± 0.55‰ and -0.07 ± 0.16‰, respectively). Interval V spans the latest Hirnantian to Rhuddanian stages (the upper part of *Metabolograptus persculptus* graptolite zone to the *Parakidograptus acuminatus* graptolite zones). Negative δ^{202}Hg and negative to near-zero Δ^{199}Hg values were observed in this interval at QL (-0.12 ± 0.27‰ and 0.05 ± 0.12‰, respectively) and TB (-0.23 ± 0.58‰ and 0.02 ± 0.10‰, respectively).

DISCUSSION

Host phases of Hg across the Ordovician-Silurian Transition

Marine sediments globally have an average THg concentration of 62.4 ppb.[15] The enrichments of Hg in Intervals II-V of the two studied sections (with mean THg concentrations between 100 and 200 ppb) are consistent with previously reported Hg enrichments across the O-S transition, including sections from the USA, UK, Poland, and South China (Figure 1D). The strong Hg enrichment is well shown in the LOESS (Locally Weighted Scatterplot Smoothing) curve (Figure. S3),[8,10-13,16,23] indicating a global-scale event. THg exhibits a stronger correlation with TOC (Pearson r = 0.79, p<0.01, n=34) than with TS (Pearson r = 0.36, p<0.01, n=34) in the TB section. However, THg and TOC correlate significantly in the QL section (Pearson r = 0.62, p<0.01, n=77), as do THg and TS (Pearson r = 0.63, p<0.01, n=77) (Figure S4). Thus, it can be

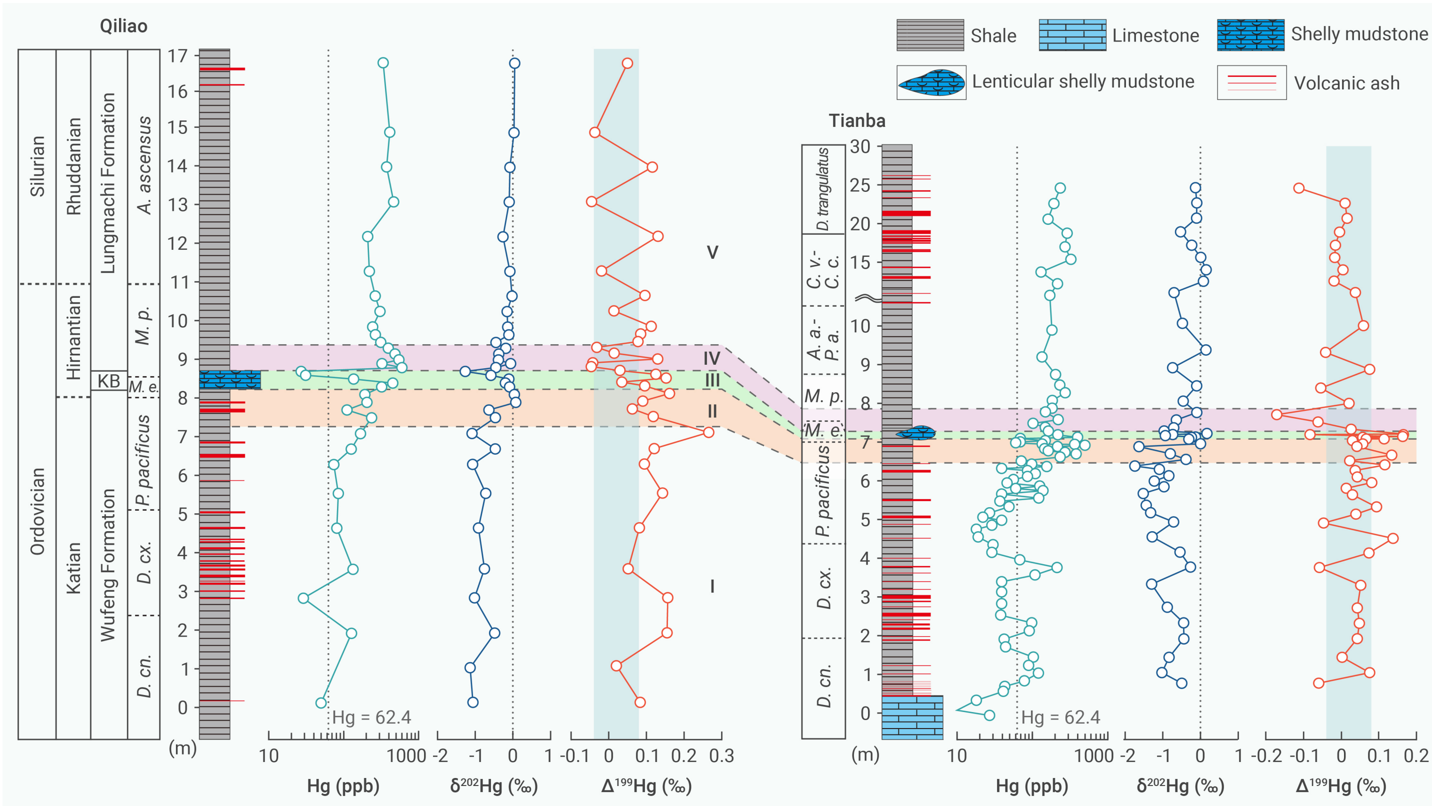

Figure 2. Comparison of Hg and Hg isotope data between the two studied sections on the Yangtze Shelf Sea in South China Hg concentration data of the QL and TB sections are from ref.[23] The light blue bars represent the range of Δ^{199}Hg values of typical volcanic (i.e., mantle-derived) Hg. Graptolite zones: *D. cn.*, *D. cx.*, *P. pacificus*, *M. e.*, *M. p.*, *A. a.*, and *P. a.* as in Figure 1; *C. v.—Cystograptus vesiculosus; C. c.—Coronograptus cyphus; D. triangulatus—Demirastrites triangulatus.*

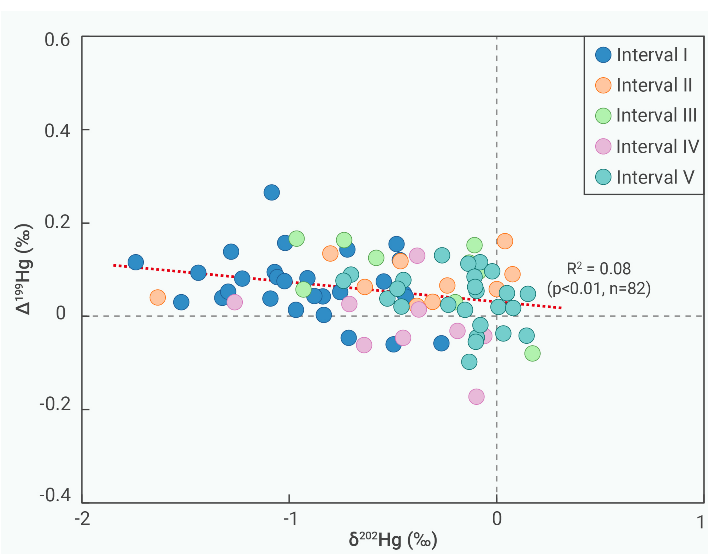

Figure 3. Crossplot of Δ^{199}Hg vs. δ^{202}Hg of QL and TB sections The red dashed line is the linear regression for all samples (slope = -0.04, R^2 = 0.08)

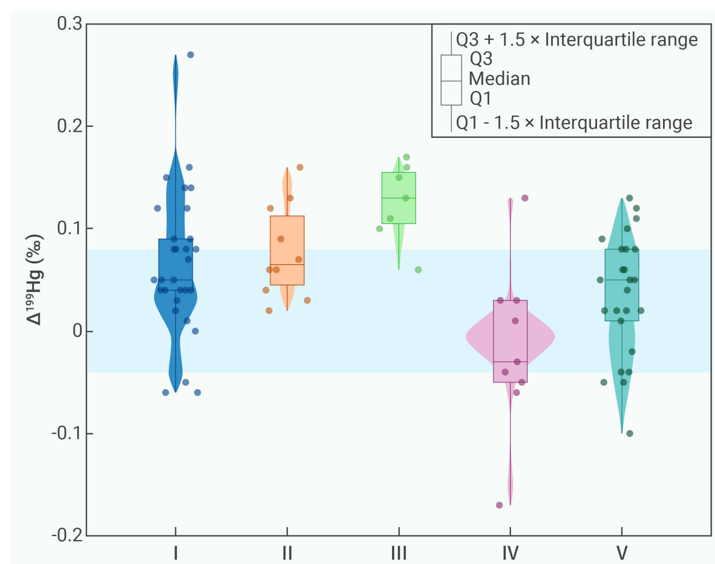

Figure 4. Violin plot of Δ^{199}Hg values for samples from Intervals I to V at the QL and TB sections The light blue bar represents the range in Δ^{199}Hg expected of volcanic Hg. The boxes represent the interquartile range (IQR), which contains the middle 50% of the data. The bottom edge of the box corresponds to the first quartile (Q1). The top edge of the box represents the third quartile (Q3). The horizontal line inside the box indicates the median of the data. Vertical lines (whisker) represent the extend to the most extreme data points that are within 1.5 times the IQR from the quartiles. The lower whisker represents extends to the smallest data point greater than or equal to Q1 − 1.5 × IQR. The upper whisker represents extends to the largest data point less than or equal to Q3 + 1.5 × IQR

concluded that organic matter and sulfides are both important hosts of Hg in the studied sections.

Multiple sources of Hg across Ordovician-Silurian Transition: implication for volcanic origin

The large variations in δ^{202}Hg (-1.26 to 0.08‰ and -1.74 to 0.17‰ at QL and TB, respectively) and Δ^{199}Hg (-0.05 to 0.27‰ and -0.17 to 0.17 at QL and TB, respectively) in the two studied sections (Figure 2) suggest fluctuations in Hg sources before, during, and after the LOME. Samples from the QL and TB sections exhibit a very weak correlation between Δ^{199}Hg and δ^{202}Hg (R^2 = 0.08, Figure 3), with a Δ^{199}Hg/δ^{202}Hg slope of -0.04. The δ^{202}Hg values may be affected by secondary processes during sedimentation, while Δ^{199}Hg demonstrates resistance to these processes. Thus, δ^{202}Hg variations cannot be directly interpreted as Hg source signals, whereas Δ^{199}Hg changes in the

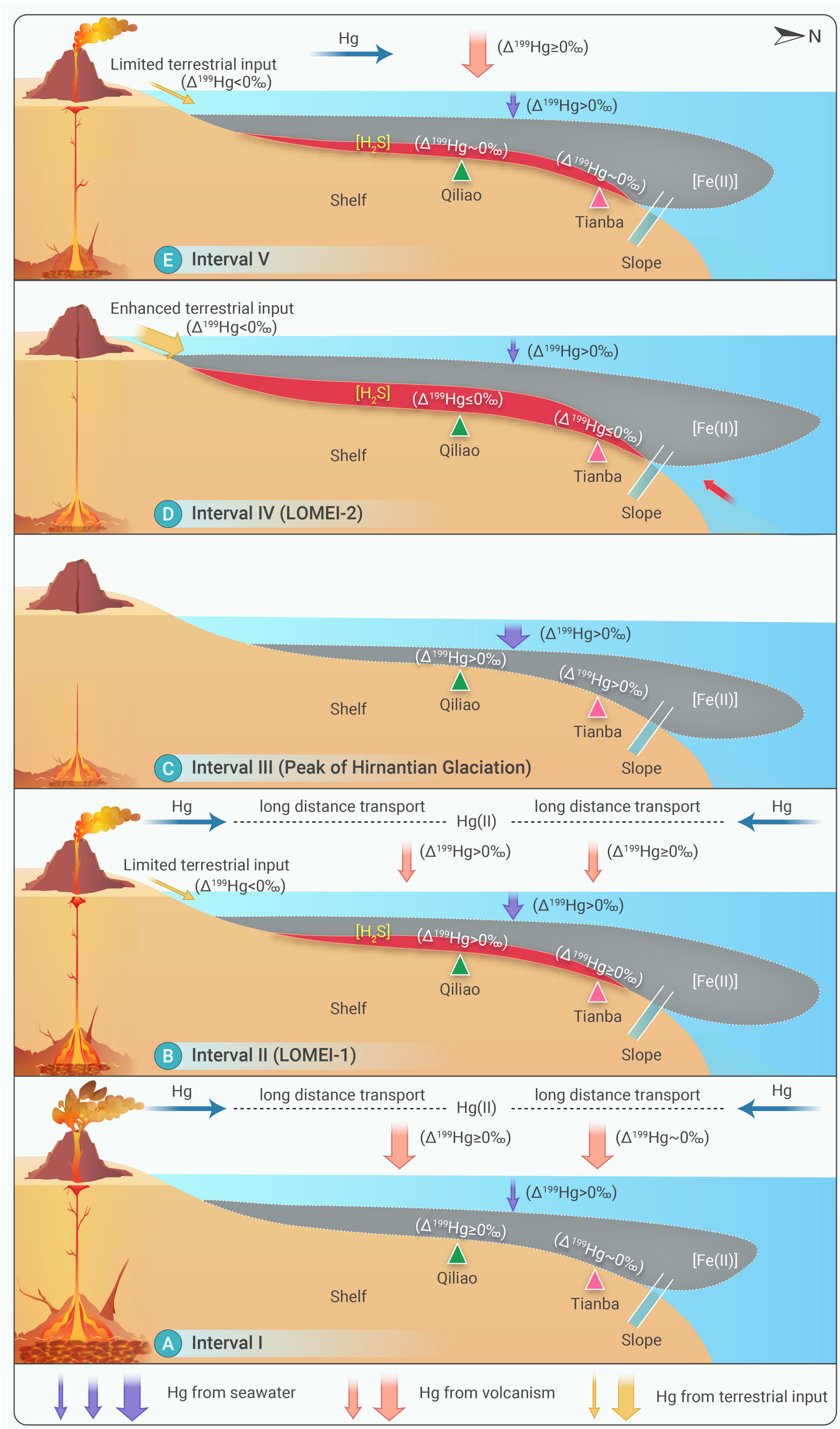

Figure 5. Schematic cartoon model illustrating the Hg cycles across the O-S transition on the Yangtze Shelf Sea in South China (redox conditions are from refs.[6,18]).

QL and TB sections likely serve as a more reliable tracer of Hg sources.

Interval I displays near-zero to slightly positive Δ^{199}Hg values (Figures 4 & S5). These values are close to those determined for Hg derived from large-scale volcanism eruptions[20] and seawater (Figure 5A), since Hg in seawater can have Δ^{199}Hg values >0 due to the long-distance transport of volcanic-sourced atmospheric Hg(II).[37] Similarly, near-zero to slightly positive Δ^{199}Hg values in Interval II, coupled with increased THg and Hg/TOC ratios (Figure S3), suggest enhanced deposition of Hg from volcanism and seawater (Figure 5B). In Interval III, the slight shift to more positive Δ^{199}Hg values (Figures 2 & 4), lower THg and Hg/TOC ratios (Figure S3) collectively suggest a lack of large volcanic eruptions during this interval, and that Hg was mainly from seawater (Figure 5C). In Interval IV, both sections show negative excursions in Δ^{199}Hg (Figures 4 & S5). The negative Δ^{199}Hg values are commonly interpreted as resulting from either a transient input of terrestrial Hg or the oxidation of atmospheric Hg^0 by sulfidic seawater within photic-zone euxinia (PZE).[38,39] The negative correlation between Δ^{199}Hg and δ^{202}Hg suggests the potential influence of PZE. However, the negative δ^{202}Hg values observed during Interval IV in the QL and TB sections (Figure 2) rule out a PZE origin, as oxidation processes within PZE typically produce positive MDF signatures (Figure 3).[38,39] Thus, the negative Δ^{199}Hg values in interval IV are more likely attributed to the terrestrial Hg input (Figure 5D), since terrestrial materials are generally characterized by negative Δ^{199}Hg values.[19] In Interval V, a return to near-zero Δ^{199}Hg values (Figures 2 & 4) and increased Hg/TOC ratios (Figure S3) suggest renewed volcanic activity during this stage (Figure 5E).

In summary, Hg from volcanism, terrestrial input, and seawater likely collectively contributed to the variations of Hg concentration and isotopic composition across the O-S transition in the studied sections. These variations provide novel evidence of significant changes in the climate-land-ocean system and associated biotic crises during the LOME, as discussed below.

Linking extensive volcanism to changes in the atmosphere-land-ocean system and LOME

The near-zero to slightly positive Δ^{199}Hg values associated with abundant volcanic ash layers in Interval I (early to late Katian stage) suggest that significant volcanic activity was ongoing prior to LOMEI-I (Interval II) (Figure 5A). Large volcanic eruptions can emit large amounts of volcanic ash and SO_2. Upon deposition into the ocean, the ash could release massive amounts of nutrients, promoting primary productivity,[6,40] which in turn resulted in oxygen consumption and deoxygenation in the water column due to the respiration of organic matter. At the same time, SO_2 has the potential to intensify ocean euxinia with the assistance of sulfate-reducing bacteria.[41] The data across the LOMEI-1 may reflect this, because Interval II is marked by a clear increase in THg that retains near-zero to slightly positive Δ^{199}Hg values (Figure 4) as well as abundant small pyrite framboids recognized in previous work, indicative of euxinic conditions.[42]

Protracted emission of volcanic ash and SO_2 in Intervals I and II create high concentrations of aerosols, leading to the backscattering of solar radiation, absorption of outgoing long-wave radiation, and disruptions in atmospheric radiative balance, eventually causing global cooling and thus perhaps driving at least in part the well-known Hirnantian glaciation in Interval III.[43-45] This cooling of the surface ocean related to this glaciation,[46,47] would lead to subsidence of cold and dense surface seawater,[48] and deposition of seawater Hg into seafloor sediments, thus resulting in positive shifts of Δ^{199}Hg in the Interval III samples. Global cooling during Interval III could have deteriorated the ecological environment for lower-latitude marine fauna (i.e. phytoplankton, zooplankton),[49,50] further enhancing the LOMEI-1 (Figure 5C).

Long-lasting volcanic eruptions through Intervals I and II would also have emitted large amounts of volcanic CO_2. Once the volcanic ash and SO_2 responsible for transient cooling were fully sequestered from the atmosphere during Interval III, the longer-term impact of sustained volcanic CO_2 inputs could have led to warming in Interval IV. This is consistent with the observed significant increase in the chemical index of alteration (CIA) during LOMEI-2 (Interval IV).[18] In this scenario, enhanced continental weathering would have led to elevated fluxes of terrestrial Hg, resulting in negative shifts of Δ^{199}Hg in Interval IV samples. Elevated fluxes of nutrients would promote oceanic productivity,[51] leading to the deoxygenation of the water column due to the remineralization of organic matter. Additionally, elevated nutrients fluxes could exacerbate euxinic conditions, as supported by the observation of pyrite framboids in Interval IV samples.[42] Collectively, euxinic ocean conditions are believed to cause the LOMEI-2 (Figure 5D).[18,42] In Interval V, the elevated Hg concentrations, near-zero Δ^{199}Hg values (Figures 2-3), and abundant volcanic ash layers suggest renewed volcanic eruptions during this stage (Figure 5E).

CONCLUSION

Our high-resolution Hg isotopes through two sections in South China across the Ordovician-Silurian (O-S) transition indicate multiple Hg sources linked to intensive volcanism. Large-scale volcanism could explain the global environmental changes across the O-S transition, including ocean euxinia and glaciation, as well as the associated LOMEI-1. Volcanism could also have triggered global warming following the Hirnantian glaciation, leading to enhanced terrestrial nutrient and sulfate fluxes to the ocean and facilitating further deoxygenation and the LOMEI-2. We thus conclude that intensive volcanism could have induced significant changes in the atmosphere-land-ocean system across the O-S transition and contributed to the associated biotic crises of the LOME.

REFERENCES

1. Sheehan P.M. (2001). The Late Ordovician mass extinction. *Annu. Rev. Earth Planet. Sci.* **29**:331–364. DOI:10.1146/annurev.earth.29.1.331
2. Melchin M.J., Mitchelll C.E., Holmden C., et al. (2013). Environmental changes in the Late Ordovician–early Silurian: Review and new insights from black shales and nitrogen isotopes. *Geol. Soc. Am. Bull.* **125**:1635–1670. DOI:10.1130/B30812.1
3. Fan J.X., Shen S.Z., Erwin D.H., et al. (2020). A high-resolution summary of Cambrian to Early Triassic marine invertebrate biodiversity. *Science* **367**:272–277. DOI:10.1126/science.aax4953
4. Harper D.A.T., Hammarlund E.U. and Rasmussen C.M.Ø. (2014) End Ordovician extinctions: A coincidence of causes. *Gondwana Res.* **25**:1294-1307. DOI: 10.1016/j.gr.2012.12.021.
5. Rong J.Y., Harper D.A.T., Huang B., et al. (2020). The latest Ordovician Hirnantian brachiopod faunas: New global insights. *Earth-Sci. Rev.* **208**:103280. DOI:10.1016/j.earscirev.2020.103280
6. Qiu Z., Zou C.N., Mills B.J.W., et al. (2022). A nutrient control on expanded anoxia and global cooling during the Late Ordovician mass extinction. *Commun. Earth Environ.* **3**:82. DOI:10.1038/s43247-022-00412-x
7. Brenchley P.J. (1984). Late Ordovician extinctions and their relationship to the Gondwana glaciation. *Geol. J.* **11**:291–315.
8. Bond D.P.G. and Grasby S.E. (2020). Late Ordovician mass extinction caused by volcanism, warming, and anoxia, not cooling and glaciation. *Geology* **48**:777–781. DOI:10.1130/G47377.1
9. Grasby S.E., and Bond D.P.G. (2023). How Large Igneous Provinces Have Killed Most Life on Earth-Numerous Times. *Elements* **19**:276–281. DOI:10.2138/gselements.19.5.276
10. Jones D.S., Martini A.M., Fike D.A., et al. (2017). A volcanic trigger for the Late Ordovician mass extinction. *Mercury data from south China and Laurentia. Geology* **45**:631–634. DOI:10.1130/G38940.1
11. Gong Q., Wang X.D., Zhao L.S., et al. (2017). Mercury spikes suggest volcanic driver of the Ordovician-Silurian mass extinction. *Sci. Rep.* **7**:5304. DOI:10.1038/s41598-017-05524-5
12. Smolarek-Lach J., Marynowski L., Trela W., et al. (2019). Mercury spikes indicate a volcanic trigger for the Late Ordovician mass extinction event: An example from a deep shelf of the Peri-Baltic Region. *Sci. Rep.* **9**:3139. DOI:10.1038/s41598-019-39333-9
13. Hu D.P., Li M.H., Chen J.B., et al. (2021). Major volcanic eruptions linked to the Late Ordovician mass extinction: Evidence from mercury enrichment and Hg isotopes. *Global Planet. Change* **196**:103374. DOI:10.1016/j.gloplacha.2020.103374
14. Percival L.M., Ruhl M., Hesselbo S.P., et al. (2017). Mercury evidence for pulsed volcanism during the end-Triassic mass extinction. *Natl. Acad. Sci. USA* **114**:7929–7934. DOI:10.1073/pnas.1705378114
15. Grasby S.E., Them T.R., Chen Z., et al. (2019). Mercury as a proxy for volcanic emissions in the geologic record. *Earth-Sci. Rev.* **196**:102880. DOI:10.1016/j.earscirev.2019.102880
16. Liu Y., Li Y.C., Hou M.C., et al. (2023). Terrestrial rather than volcanic mercury inputs to the Yangtze Platform (South China) during the Ordovician-Silurian transition. *Global Planet. Change* **220**:104023. DOI:10.1016/j.gloplacha.2022.104023
17. Hammarlund E.U., Dahl T.W., Harper D.A., et al. (2012) A sulfidic driver for the end-Ordovician mass extinction. *Earth Planet. Sci. Lett.* **331-332**:128-139. DOI: 10.1016/j.epsl.2012.02.024.
18. Zou C.N., Qiu Z., Poulton S.W., et al. (2018). Ocean euxinia and climate change "double whammy" drove the Late Ordovician mass extinction. *Geology* **46**:535–538. DOI:10.1130/G40121.1
19. Blum J.D., Sherman L.S., and Johnso M.W. (2014). Mercury isotopes in earth and environmental sciences. *Annu. Rev. Earth Planet. Sci.* **42**:249–269. DOI:10.1146/annurev-earth-050212-124107
20. Yin R.S., Chen D., Pan X., et al. (2022). Mantle Hg isotopic heterogeneity and evidence of oceanic Hg recycling into the mantle. *Nat. Commun.* **13**:948. DOI:10.1038/s41467-022-28577-1
21. Yin R.S., Wang X.Y., Sun R.Y., et al. (2024). Linking the mercury biogeochemical cycle to the deep mercury cycle: A mercury isotope perspective. *Chem. Geol.* **654**:122063. DOI:10.1016/j.chemgeo.2024.122063
22. Lu Y.B., Shen J., Wang Y.X., et al. (2022). Seawater sources of Hg enrichment in Ordovician-Silurian boundary strata, South China. *Palaeogeogr. Palaeoclimatol. Palaeoecol.* **601**:111156. DOI:10.1016/j.palaeo.2022.111156
23. Qiu Z., Wei H.Y., Tian L., et al. (2022). Different controls on the Hg spikes linked the two pulses of the Late Ordovician mass extinction in South China. *Sci. Rep.* **12**:5195. DOI:10.1038/s41598-022-08941-3
24. Chen X., Rong J.Y., Li Y., et al. (2004). Facies patterns and geography of the Yangtze region, South China, through the Ordovician and Silurian transition. *Palaeogeogr. Palaeoclimatol. Palaeoecol.* **204**:353–372. DOI:10.1016/S0031-0182(03)00736-3
25. Su W.B., Huff W.D., Ettensohn F.R., et al. (2009). K-bentonite, black-shale and flysch successions at the Ordovician-Silurian transition, South China: Possible sedimentary responses to the accretion of Cathaysia to the Yangtze Block and its implications for the evolution of Gondwana. *Gondwana Res.* **15**:111–130. DOI:10.1016/j.gr.2008.06.004
26. Qiu Z. and Zou C.N. (2020). Controlling factors on the formation and distribution of "sweet-spot areas" of marine gas shales in South China and a preliminary discussion on unconventional petroleum sedimentology. *J. Asian Earth Sci.* **194**:103989. DOI:10.1016/j.jseaes.2019.103989
27. Qiu Z., Liu B., Lu B., et al. (2022). Mineralogical and petrographic characteristics of the Ordovician-Silurian Wufeng-Longmaxi Shale in the Sichuan Basin and implications for depositional conditions and diagenesis of black shales. *Mar. Petrol. Geol.* **135**:105428. DOI:10.1016/j.marpetgeo.2021.105428
28. Qiu Z., Li Y.F., Xiong W., et al. (2023). Revisiting paleoenvironmental changes on the Upper Yangtze Block during the Ordovician-Silurian transition: New insights from elemental geochemistry. *Sediment. Geol.* **450**:106377. DOI:10.1016/j.sedgeo.2023.106377
29. Guo X.W., Luo T., Dong T., et al. (2023). Quantitative estimation on methane storage capacity of organic-rich shales from the Lower Silurian Longmaxi Formation in the Eastern Sichuan Basin, China. *J. Earth Sci.* **34**:1851–1860. DOI:10.1007/s12583-020-1394-7
30. Zou C.N., Qiu Z., Zhang J.Q., et al. (2022). Unconventional petroleum sedimentology: A key to understanding unconventional hydrocarbon accumulation. *Engineering* **18**:62–78. DOI:10.1016/j.eng.2022.06.016
31. Qiu Z., and Zou C.N. (2020). Unconventional petroleum sedimentology: Connotation and prospect. *Acta Sedimentologica Sinica* **38**:1–29. DOI:10.14027/j.issn.1000-0550.2019.116
32. Du X.B., Jia J.X., Zhao K., et al. (2021). Was the volcanism during the Ordovician-Silurian transition in South China actually global in extent. *Evidence from the distribution of volcanic ash beds in black shales. Mar. Pet. Geol.* **123**:104721. DOI:10.1016/j.marpetgeo.2020.104721
33. Wang G.X., Zhan R.B. and Percival I.G. (2019). The end-Ordovician mass extinction: A single-pulse event. *Earth-Sci. Rev.* **192**:15–33. DOI:10.1016/j.earscirev.2019.01.023
34. Yin R.S., Krabbenhoft D.P., Bergquist B.A., et al. (2016). Effects of Mercury and

Thallium concentrations on high precision determination of Mercury isotope composition by Neptune plus multiple collector inductively coupled plasma mass spectrometry. *J. Anal. Atom. Spectrom.* **31**:2060–2068. DOI:10.1039/C6JA00107F
35. Zerkle A.L., Yin R.S., Chen C.Y., et al. (2020). Anomalous fractionation of mercury isotopes in the Late Archean atmosphere. *Nat. Commun.* **11**:1709. DOI:10.1038/s41467-020-15495-3
36. Blum J.D. and Bergquist B.A. (2007). Reporting of variations in the natural isotopic composition of mercury. *Anal. Bioanal. Chem.* **388**:353–359. DOI:10.1007/s00216-007-1236-9
37. Štrok M., Baya P.A. and Hintelmann H. (2015). The mercury isotope composition of Arctic coastal seawater. *C.R. Geosci.* **347**:368–376. DOI:10.1016/j.crte.2015.04.001
38. Liu M., Yuan W., Fang C.G., et al. (2024). Mercury isotope evidence for Middle Ordovician photic-zone euxinia: Implications for termination of the Great Ordovician biodiversification event. *Gondwana Res.* **137**:131–144. DOI:10.1016/j.gr.2024.09.008
39. Zheng W., Zhou A.W., Sahoo S.K., et al. (2023). Recurrent photic zone euxinia limited ocean oxygenation and animal evolution during the Ediacaran. *Nat. Commun.* **14**:3920. DOI:10.1038/s41467-023-39427-z
40. Zhao K., Du X.B., Lu Y.B., et al. (2020). Is volcanic ash responsible for the enrichment of organic carbon in shales. *Quantitative characterization of organic-rich shale at the Ordovician-Silurian transition. Geol. Soc. Am. Bull.* **133**:837–847. DOI:10.1130/B35737.1
41. Hu D.P., Li M.H., Zhang X.L., et al. (2020). Large mass-independent sulphur isotope anomalies link stratospheric volcanism to the Late Ordovician mass extinction. *Nat. Commun.* **11**:2297. DOI:10.1038/s41467-020-16228-2
42. Zou C.N., Qiu Z., Wei H.Y., et al. (2018). Euxinia caused the Late Ordovician extinction: Evidence from pyrite morphology and pyritic sulfur isotopic composition in the Yangtze area, South China. *Palaeogeogr. Palaeoclimatol. Palaeoecol.* **511**:1–11. DOI:10.1016/j.palaeo.2017.11.033
43. Schoene B., Eddy M.P., Samperton K.M., et al. (2019). U-Pb constraints on pulsed eruption of the Deccan Traps across the end-Cretaceous mass extinction. *Science* **363**:862–866. DOI:10.1126/science.aau2422
44. Robock A. (2000). Volcanic eruptions and climate. *Rev. Geophys.* **38**:191–219. DOI:10.1029/1998RG000054
45. Ernst E.R. and Youbi N. (2017). How Large Igneous Provinces affect global climate, sometimes cause mass extinctions, and represent natural markers in the geological record. *Palaeogeogr. Palaeoclimatol. Palaeoecol.* **478**:30–52. DOI:10.1016/j.palaeo.2017.03.014
46. Trotter J.A., Williams I.S., Barnes C.R., et al. (2008). Did cooling oceans trigger Ordovician biodiversification. *Evidence from conodont thermometry. Science* **321**:550–554. DOI:10.1126/science.1155814
47. Finnegan S., Heim N.A., Peters S.E., et al. (2012). Climate change and the selective signature of the Late Ordovician mass extinction. *Proc. Natl. Acad. Sci. USA* **109**:6829–6834. DOI:10.1073/pnas.1117039109
48. Rahmstorf S. (2002). Ocean circulation and climate during the past 120,000 years. *Nature* **419**:207–214. DOI:10.1038/nature01090
49. Brenchley P.J., Marshall J.D. and Underwood C.J. (2001). Do all mass extinctions represent an ecological crisis. *Evidence from the Late Ordovician. Geol. J.* **36**:329–340. DOI:10.1002/gj.880
50. Crampton J.S., Coopera R.A., Sadlerc P.M., et al. (2016). Greenhouse icehouse transition in the Late Ordovician marks a step change in extinction regime in the marine plankton. *Proc. Natl. Acad. Sci. USA* **113**:1498–1503. DOI:10.1073/pnas.1519092113
51. Longman J., Mills B.J.W., Manners H.R., et al. (2021). Late Ordovician climate change and extinctions driven by elevated volcanic nutrient supply. *Nat. Geosci.* **14**:924–929. DOI:10.1038/s41561-021-00855-5

FUNDING AND ACKNOWLEDGMENTS

We thank Prof. Runsheng Yin and the three anonymous referees for their constructive comments which greatly contributed to improving this paper. We are also grateful to Prof. Wenjiao Xiao for his valuable comments and insightful discussions. This work was financially supported by the National Natural Science Foundation of China (Grant 42222209). The funders had no role in study design, data collection and analysis, decision to publish, or preparation of the manuscript.

AUTHOR CONTRIBUTIONS

Zhen Qiu and Caineng Zou designed research; Zhen Qiu, Weiliang Kong and Jiaqiang Zhang collected samples; Weiliang Kong measured samples; Zhen Qiu, Weiliang Kong, Qin Zhang, and Wen Liu analyzed the data; David B. Kemp, Stephen E. Grasby and Caineng Zou helped improve the manuscript; Zhen Qiu acquired funding support for this work. Zhen Qiu, Weiliang Kong, and Jiaqiang Zhang wrote the manuscript. All authors contributed to the manuscript and approved the final version.

DECLARATION OF INTERESTS

The authors declare no competing interests, financial or otherwise.

DATA AND MATERIALS AVAILABILITY

All data are available in the supplementary materials.

SUPPLEMENTAL INFORMATION

It can be found online at https://doi.org/10.59717/j.xinn-geo.2024.100124